Floods on alluvial fans: implications for reworking rates, morphology and fan hazards

A. S. Leenman[1,2], B. C. Eaton[1], and L. G. MacKenzie[3]

[1]Department of Geography, University of British Columbia, Vancouver BC, Canada
[2]School of Geography and Environment, University of Oxford, Oxford, UK
[3]Department of Forest Resources Management, University of British Columbia, Vancouver BC, Canada

Key Points:

- Experiments with the same mean flow but different hydrograph shapes generated alluvial fans with different slopes
- Rates of lateral migration and geomorphic change increased non-linearly with the flow, so that small changes to hydrograph shape had a meaningful impact on flood response
- A single, constant flow is inappropriate to represent the wide range of flows on natural fans

---

This manuscript was re-submitted to *JGR: Earth Surface* in November 2020 after a round of peer-review; subsequent versions of the manuscript may differ. If accepted, this page will be updated with a DOI for the published manuscript.

The data associated with this paper will be published on the Canadian Federated Research Data Repository, at https://doi.org/10.20383/102.0482.

Contact the corresponding author via email at anya.leenman@chch.ac.ox.uk.

Corresponding author: Anya Leenman, `anya.leenman@chch.ox.ac.uk`

Abstract

Flood events are the agents of change on alluvial fans. However, most alluvial fan experiments have used constant flows to model fans and the channels upon them. Here, we present results from a series of alluvial fan experiments with different patterns of flow variation (i.e. different hydrograph shapes). We conducted experiments with 1) constant flow, 2) alternating high and low flows, 3) a moderate flood peak that decayed slowly, alternating with a constant low flow, and 4) a high flood peak that decayed rapidly, alternating with a constant low flow. We found that different hydrographs generated fans with different slopes, even though all experiments had the same mean flow and sediment supply. In addition, higher peak flows led to increased lateral migration rates and increased erosion and deposition. These results challenge the notion that a single representative flow can be used to approximate the geomorphic effects of a range of flows in a natural stream. Moreover, our findings indicate that hydrograph shape can govern the geomorphic impact of a flood event. This means that altered basin hydrology (for instance, through changes to land cover) likely exerts an important impact on geomorphic change and natural hazards on alluvial fans.

Plain Language Summary

The steep streams that flow down alluvial fans experience a wide range of high and low flows. Here, we use a series of experiments with a small-scale model of a fan to explore the importance of this flow variability. We show how the type of flow variability influences hazards such as stream bank erosion, or the rapid inundation of areas that were previously dry. Our results suggest that when high flows occur in these steep streams, their size and duration control their impact on the stream channel. Anything that changes the size and duration of high flows (for instance, a change to the landscape upstream) could alter the severity of future flood impacts.

1 Introduction

Flood events drive change on alluvial fans. Although geomorphic change is not negligible in the intervening low or moderate flows (i.e. 'secondary processes'; Blair and McPherson (1994b); Vincent et al. (In revision)), it is high-flow events that tend to drastically rework fan morphology by reshaping or redirecting channels — often with catastrophic consequences for people or infrastructure on those fans (Beaumont & Oberlander, 1971; Church & Jakob, 2020; Field, 2001; Gutiérrez et al., 1998; Jakob et al., 2016, 2017; Larsen et al., 2001; Pearthree et al., 2004; Santo et al., 2015; Yumuang, 2006). In addition to reworking fan morphology, flood events and other primary processes (such as debris flows) transport large volumes of sediment onto fans. As a result, flood events with high sediment concentration are one of the main processes that build up alluvial fans.

'Flood' carries alternative meanings across different contexts and applications. In this paper, we consider the effects of flood 'events' — that is, sudden and short-term increases in flow above a background value. We are interested in flow *variability* over a reasonably short time: what is the effect of a rapid increase in flow, and of the shape of the flood hydrograph? Consequently, when we refer to high flows or flood events, we are not referring to a particular flood magnitude or recurrence interval. Rather, we are referring to the temporary increase in flow typically triggered by a heavy rainfall event. The geomorphic effects of such temporal flow variation, over a series of repeated flood events, are the focus of this paper.

Despite the importance of variable flow in shaping fans, experimental models of alluvial fans have generally used constant flow (Clarke et al., 2010; Delorme et al., 2017, 2018; Van Dijk et al., 2012; Schumm et al., 1987; Whipple et al., 1998; Reitz & Jerolmack, 2012; Reitz et al., 2010). This practice rests upon the assumption that a 'representative' flow rate can be used to approximate the range of flows that occur in a stream. These constant flow experiments have provided a nuanced and invaluable understanding of autogenic dynamics on alluvial fans. Nevertheless, a constant flow represents an environmental scenario that is unlikely in natural streams. Although the practice of using a single constant flow is common, it is not entirely clear how much information is lost by substituting a single flow for a range of flows; that is, how this practice might cause over- or under-estimation of geomorphic process rates in natural systems.

Conceptual work and statistical modeling have suggested that a single flow rate (discharge) may not accurately represent the dynamics of the full range of flows. For instance, Eaton (2013) noted that different aspects of river morphology (e.g. the banks or the bed surface) may be shaped by floods of different frequencies, so that there are likely multiple 'formative' discharges for a given channel. Similarly, Church and Ferguson (2015) emphasized that it is difficult to define a single flow that (over time) creates the same morphology and sedimentology as a range of natural flows, because different processes or geomorphic features have different (and non-linear) relations with discharge. The utility of the 'formative' flow was further eroded in statistical modeling by S. L. Davidson and Eaton (2018), who compared a traditional regime model of channel geometry (with constant flow) to a stochastic model with variable flood sizes. They showed that, as the variability of flood sizes increased, the channel geometry became more different from that produced by a single discharge in the regime model. Collectively, these works demonstrate the difficulty of selecting a single flow as representative. Moreover, they highlight some biases which may arise from the temporal averaging of a range of flows to give a single representative flow.

In the past five years, experiments have demonstrated that variable flow affects the morphology and evolution of fan-deltas. For instance, an experiment by Ganti et al. (2016) with variable flow produced fan-delta morphology and avulsion dynamics that differed from their experiment with constant flow. Similarly, Barefoot et al. (2021) compared constant flow and two different hydrographs, with channel dynamics and delta morphology scaling non-monotonically with flood intensity. Miller et al. (2019) compared experiments with variable flow to a constant 'flood' flow, and found that variable flow favored the construction of larger deltas with faster progradation rates. Moreover, experiments by Piliouras et al. (2017) showed that on vegetated fan-deltas, variable flow generated fan-deltas with different morphology and vegetation growth patterns, and altered flow-vegetation interactions. Collectively, these experiments highlight how, at least on fan-deltas, using variable flow not only affects morphology, but also the dynamics of channels and of natural hazards such as avulsion.

In light of the experimental evidence and issues described above, we evaluate the distortions introduced through averaging the flow to alluvial fans. We present data from four fan experiments with differing magnitudes of flow variability. Using these data, we investigate the influence of delivering the same volume of water through different hydrograph shapes. We quantify the impact of the repeated hydrographs by examining their effects on fan gradient, lateral channel migration, and geomorphic change (i.e. erosion and deposition). We reflect on the implications of our research for flood hazards on natural fans and for notions of representative discharge. Lastly, we consider the implications of our findings for stream responses to environmental change.

2 Methods

2.1 Model set-up

We conducted four experiments using a physical model of a generic gravel-cobble alluvial fan. These experiments were run in a stream table at the University of British Columbia's Biogeomorphology Experimental Laboratory. The stream table measured 2.44

× 2.44 × 0.3 m (Figure 1). Water and sediment were delivered to the fan apex through a 0.2 × 0.5 × 0.3 m feeder channel at one corner. Water was input from a constant head tank for experiments with constant flow, or from a variable head tank, monitored by a pressure sensor, for the runs with decaying flood peaks. A sediment feeder delivered sediment via a rotating pipe; the feed rate was set by the inclination of the pipe. Sediment and water inputs were mixed in a funnel and then dropped into the experiment at the head of the feeder channel. We allowed sediment to aggrade and degrade freely in the feeder channel, to mimic sediment supply buffering in a bedrock confined reach upstream of a natural fan.

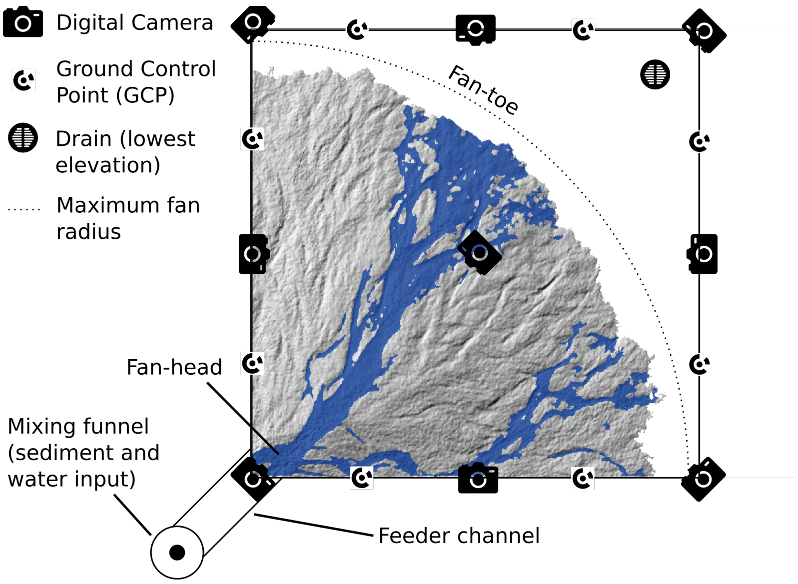

Figure 1. Experimental setup (not to scale). Water and sediment were mixed in the funnel and dropped into the head of the feeder channel, where sediment could aggrade and degrade. The hillshaded topography and flow map example are from Run 1 repeat 1 at 19 hours, 9 minutes.

We set the stream table slope to 0.0002 m m^{-1} (0.02 %) to generate flow across the table to the drain. To roughen the boundary, we glued 2 mm sand grains and Lego sheets to the base and walls of the table. We dyed the water in the experiment blue in order to apply image analysis techniques to automatically map the flow from photographs.

We collected data using an adaptation of Structure-from-Motion photogrammetry. The data collection system and its spatial accuracy are described in detail in Leenman and Eaton (2021) and Leenman (2021); here we give a brief summary. We mounted nine digital single-lens reflex cameras above the stream table to 'view' the experiment from different angles (Figure 1). All cameras captured photos synchronously; in the experiments with flood events, the first photo was always ~30 seconds after the start of the flood (see Figure 2). We glued eight 'ground control points' (GCPs) to the table walls, allowing us to georeference the photos to a local coordinate system. Each set of nine photos was processed in "AgiSoft PhotoScan Professional" (2018) to generate a topographic point cloud (~280,000 points per m^2) and co-registered orthophoto (1 mm resolution).

2.2 Experimental Scenarios

We conducted four experimental runs, each with different flow conditions. Run 1 had constant flow; Runs 2–4 had periodically repeating flood events. For Runs 2–4, each flood event lasted five minutes and was followed by a five-minute low-flow period. We repeated this 10-minute high-to-low flow cycle for the whole experiment. The flow cycle length was not scaled to a specific time-period or natural cycle, as the experiments were designed to explore the effects of the magnitude, rather than frequency, of flow oscillations.

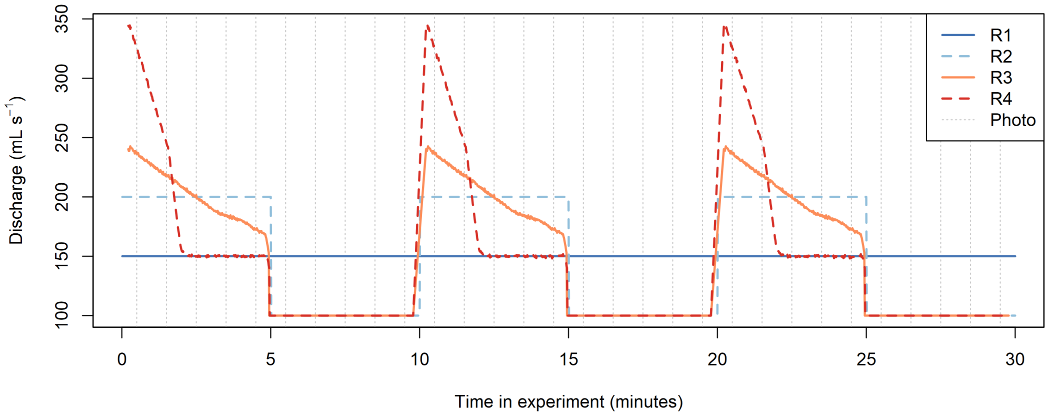

Figure 2. Flow rates for each experiment; the 10-minute high-to-low flow cycles shown here were repeated continuously. The mean flow and the total water input in a 10-minute cycle was the same in all experiments.

The hydrographs for each experiment are shown in Figure 2. Run 2 had 'flat' flood hydrographs, with a constant flood flow of 200 mL s^{-1}. Run 3 had a low flood peak of ~240 mL s^{-1}, that decayed slowly. Run 4 had a high flood peak of ~340 mL s^{-1}, that decayed rapidly. All variable flow experiments (Runs 2–4) had a constant low flow of 100 mL s^{-1} for five minutes between the flood events.

One of our aims was to investigate the impact of temporally averaging flow to the fan. We therefore designed the experiments so that in Run 1, all flow variability was averaged out to produce a constant flow of 150 mL s^{-1}, equal to the mean flow in Runs 2–4. The total volume of water delivered in each 10-minute period (the high-to-low flow cycle) was therefore equal across all four experiments. Moreover, in Runs 2–4, each flood peak contained the same volume of water, but with a different temporal distribution in the different experiments. This arrangement allowed us to test the impact of averaging the flow *within* a flood event: in Run 2, we averaged out the decaying flood hydrographs of Runs 3 and 4, instead using a constant flood flow equal to the mean flood flow in Runs 3 and 4.

In all experiments, the sediment supply to the feeder channel was constant at 5 g s^{-1}. Sediment concentration, then, was determined by the flow variations. Because we allowed sediment to aggrade and degrade freely in the feeder channel, the effective sediment feed rate (and sediment concentration) could readily adjust in response to flow variation, through cutting or filling of the sediment stored in the feeder channel. This process was designed to mimic the behavior of the steep, confined streams that typically feed alluvial fans.

Using a length scale of 1:128, we approximated the experimental grain size distribution (GSD) from a surface gravel sample collected on Three Sisters Creek fan, Canmore, Canada. Compared to most fan experiments, our sediment mixture was widely graded. The experimental GSD ranged from 0.25 mm to 8 mm, and 95% of the mixture was finer than 2.3 mm (Figure 3). Visual observations suggest the mixture was primarily transported as bedload. Subsurface flow through the sandy mixture allowed seepage channels to form, which have been observed on natural fans; for instance, phenomena such as downfan channel narrowing and spring formation have been attributed to infiltration on fans (S. K. Davidson et al., 2013; Kesel & Lowe, 1987; Woods et al., 2006).

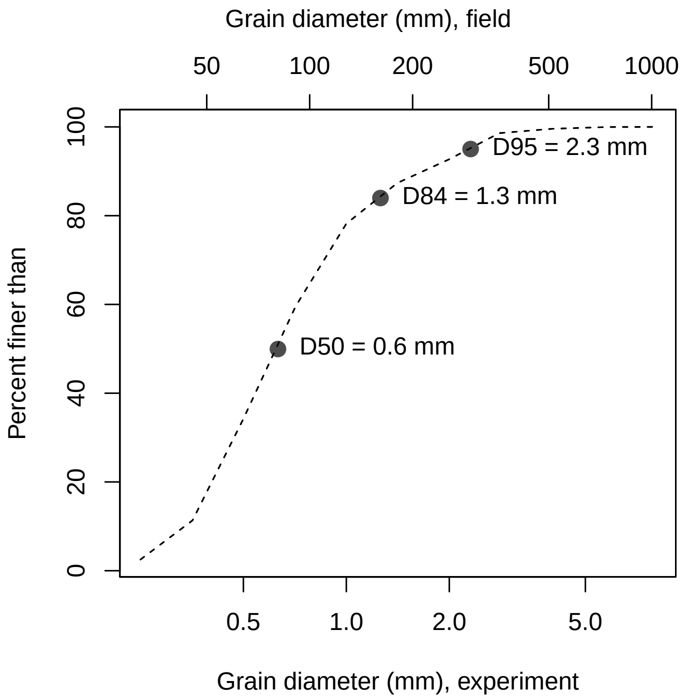

Figure 3. The grain size distribution (GSD) of our experimental sediment mixture.

We ran each experiment for ~20 hours, until the fan prograded to the stream table edges. For each experiment, we then ran two additional repeats. Unless otherwise stated, our figures show data from all three repeats of the experiment(s).

2.3 Experimental Approach

Our experimental fan is a 'similarity-of-process' model or 'analog' model (c.f. Hooke (1968a); Paola et al. (2009)), as are most physical models of alluvial fans and fan-deltas (Bryant et al., 1995; Clarke et al., 2010; Davies & Korup, 2007; Delorme et al., 2017, 2018; Van Dijk et al., 2009; De Haas et al., 2016, 2018; Hamilton et al., 2013; Hooke, 1967, 1968b; Hooke & Rohrer, 1979; Miller et al., 2019; Piliouras et al., 2017; Reitz & Jerolmack, 2012; Schumm et al., 1987). In our model, flow reshapes the fan through the erosion, transport and deposition of sediment, thereby incorporating the key formative processes on natural fans. Because we use the 'similarity-of-process' approach, we do not attempt to extrapolate the rates or volumes of our findings to the field. Instead, comparisons between our different experiments demonstrate how natural fans are likely to respond to different scales of flow variability. Such comparisons also highlight the distortions introduced through the flow averaging we impose in Runs 1 and 2.

In alluvial fan models, it is difficult to meet the Froude scaling requirements described by Peakall et al. (1996) due to the large geometric scaling ratio required to build a conveniently small laboratory fan. In our experiments it was not possible to even control the Froude (Fr) or Reynolds (Re) numbers, as the fan's slope and channel dimensions were entirely self-formed. We have estimated these parameters for the fan-head (where flow was generally confined to a single channel), based on estimated flow width, depth and velocity; see Table S1 in the Supplementary Information (SI) for the values used to estimate these dimensionless numbers. Estimated Fr was 1.3–2.6, depending on the flow. These supercritical values match observations during floods on natural fans (Beaumont & Oberlander, 1971; Rahn, 1967). Farther downfan, flow likely became subcritical as it spread into multiple distributaries. Using the D_{84} as a representative grain size, we estimated particle Reynolds numbers (Re^*) of 57–76 (depending on the flow), which conform to the threshold of 15 proposed by Parker (1979) and Ashworth et al. (1994), and also conform to the minimum of 70 recommended by Schlichting and Gersten (2016) and Yalin (1971) for some flows. We estimated Re of 670–2,330, indicating that flow was generally in the transitional regime between laminar and turbulent flow (preventing the attainment of Froude similarity). Many other experimental fan studies also reported flows that were not fully turbulent (Davies et al., 2003; Davies & Korup, 2007; Delorme et al., 2017, 2018; Van Dijk et al., 2012; Guerit et al., 2014; Hamilton et al., 2013; Reitz et al., 2010; Reitz & Jerolmack, 2012; Whipple et al., 1998). Although those models operated outside of Froude similarity, they were found to successfully reproduce the fan-channel dynamics that are of interest to us.

2.4 Data Processing and Analysis

Our photogrammetric data collection system generated a topographic point cloud and 1 mm resolution orthophoto for each minute of the experiments. These two data products formed the basis for all subsequent analysis, which was conducted in R (R Core Team, 2021) with extensive use of the *Raster* package (Hijmans, 2020). All analyses were limited to areas of the fan that had aggraded to > 6 mm above the initial empty table surface, so that surface scum over the drain was not captured in our topographic change detection.

To analyze the orthophotos, we applied a color filter to map the flow pattern (water was dyed blue in the experiments; see SI for further detail on the flow map generation). We performed change detection between the flow maps (Figure 4), to measure rates of lateral migration and quantify the area affected by channel reorganization events such as avulsion. Specifically, we measured the area newly inundated in each minute, and expressed it as a percentage of fan area at time (t), as follows:

$$F_n(t) \ = \frac{Area\ newly\ inundated\ in\ previous\ minute}{Fan\ area\ (t)} * 100 \tag{1}$$

We also measured the area newly abandoned by flow in each minute, expressed as follows:

$$F_a(t) \ = \frac{Area\ newly\ abandoned\ in\ previous\ minute}{Fan\ area\ (t)} * 100 \tag{2}$$

To analyze the topographic data, we generated 1 mm resolution digital elevation models (DEMs) from the point clouds using nearest neighbor interpolation. The DEMs allowed us to quantify fan gradient: for every DEM, we extracted 88 radial downfan profiles, and measured gradient as the slope of a linear regression of elevation against distance from the fan-head (profiles were quasi-linear; see Figure S1 (SI) for examples).

We also subtracted successive DEMs to generate 'DEMs of Difference' (DoDs); we first smoothed the DEMs with a 7 × 7 mm moving average filter to reduce grain-scale noise. The DoDs allowed us to quantify the volume of erosion and deposition that occurred between each DEM. Erosion or deposition of < 2 mm was discounted as noise and removed from all DoDs. An error analysis for Run 1 estimated with 90% confidence that cell elevations varied by less than -0.7 mm, +0.8 mm over any 30-minute period (see p. 130-131 in Leenman (2021)) so this error threshold was conservative and eliminated most noise in the DoDs. We then summed the erosion or deposition across each DoD,

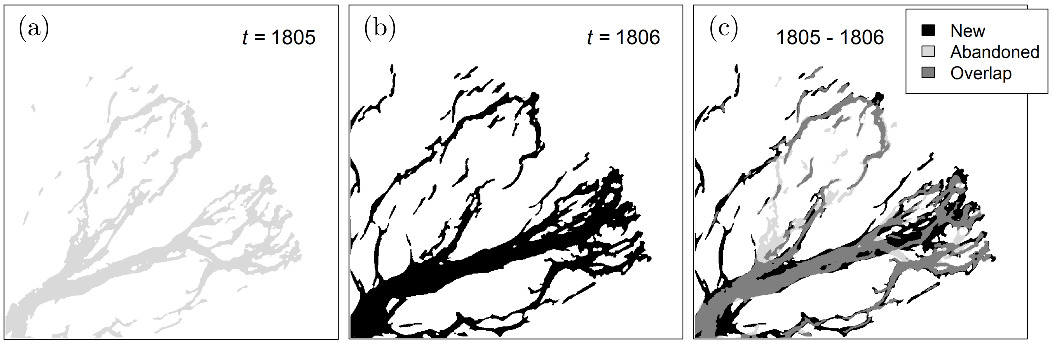

Figure 4. Change detection between successive flow maps. Panels show the flow pattern at 1805 (a) and a minute later at 1806 (b) and then the change detection between them (c). Areas shaded black in (c) correspond to the *'Area newly inundated'* in equation 1; areas shaded pale gray in (c) correspond to the *'Area newly abandoned'* in equation 2. Data from Run 3 repeat 1.

to provide a total volume of erosion (V_e) or deposition (V_d) for that minute of the experiment. Finally, we summed the absolute values of V_e and V_d to give a metric for the total volume of geomorphic change (M) in each minute:

$$M(t) = |V_e(t)| + |V_d(t)| \tag{3}$$

The DoDs occasionally produced unrealistically large values of M, due to noise in the DEMs. These outliers were identified visually by plotting M against the time in each high-to-low flow cycle (as in Figure 9 in our results) and then manually checking those DoDs. Based on this inspection, we set an outlier-removal threshold for each run and applied it to all repeats of that experiment.

Summing M across each complete DoD did not allow us to explore spatial patterns of topographic change. In order to explore these spatial patterns in the flood events and low-flow periods of Runs 2–4, we generated five-minute DoDs (again first smoothing with a 7 × 7 mm moving window) by subtracting the first and last DEM in each (e.g. $t5-t0$ for flood events, and $t10-t5$ for low-flow periods). We then extracted seven equally-spaced downfan profiles from each five-minute DoD. These profiles allowed us to explore how the downfan distribution of erosion and deposition was different in flood events and the intervening low-flow periods.

In this paper, we present and analyze all data from 12 hours of experimental running time and onward. Following Leenman and Eaton (2021), we exclude data from earlier in the experiments, as fan morphology and dynamics appeared to be scale dependent prior to this cutoff. In particular, fan slope and wetted fraction (inundated area / total fan area) were related to fan size until this later period of the experiment (Leenman & Eaton, 2021).

3 Results

To gain a general understanding of how our experiments behaved, we encourage readers to view the experimental time-lapse videos: `https://youtu.be/ML2LV28MQEM` (**Run 1**), `https://youtu.be/_OwWnb39PYE` (**Run 2**), `https://youtu.be/NxVGxepg4BQ` (**Run 3**), and `https://youtu.be/1ua_whH9jME` (**Run 4**). Additional time-lapses, with frames captured at a higher frequency, were generated for **Run 3** (`https://youtu.be/L-27xGWeOCw`) and **Run 4** (`https://youtu.be/NY5E_jxee2E`). Links to these videos are also given in Table S2 (SI).

Flow on the fans was highly dynamic; channels formed and re-formed in just a few minutes, and channel reorganization was frequent. The flow pattern was almost always multi-threaded. For the runs with floods, the start of the flood peak typically increased the fraction of the fan covered by flow, often causing flow pattern divergence. The areal extent of inundation was larger when the flood peak was larger (Figure 5, upper panel). Often, this inundation also rearranged flow patterns (i.e. triggered avulsion). Later in each flood event, channels adjusted through rapid lateral migration. When flow dropped to 100 mL s^{-1} in the low-flow periods, flow at first occupied the channel pattern set by the previous flood event (Figure 5, lower panel). Channel pattern then adjusted throughout the low-flow period, via slower lateral migration.

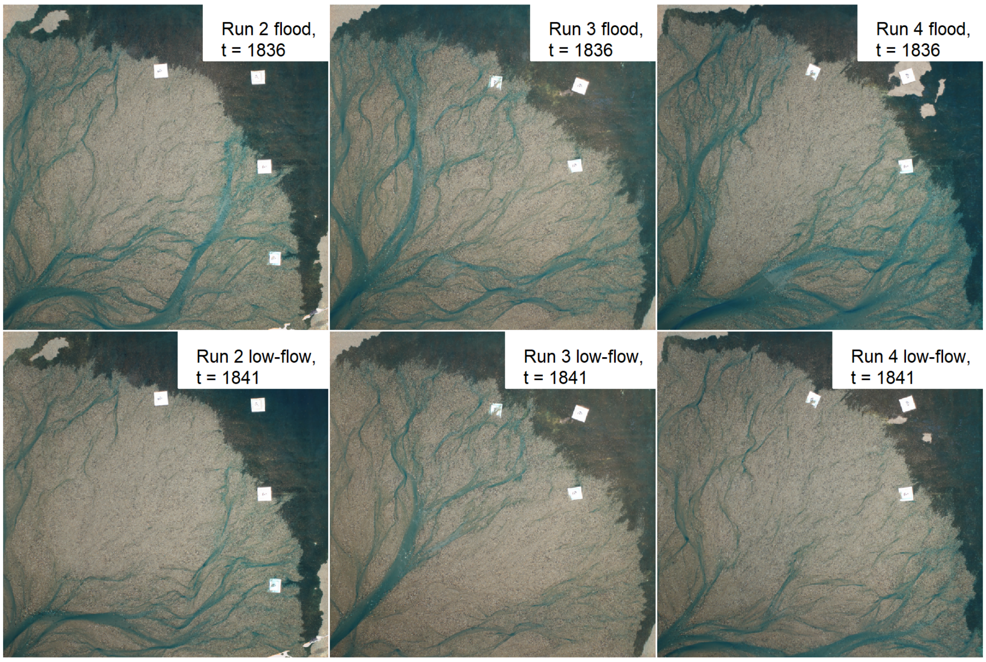

Figure 5. Examples of fan inundation at the beginning of a flood event (upper panel) and the beginning of the following low-flow period (lower panel). The flood peak flow increases from left to right. Data are from Run 2 repeat 3, Run 3 repeat 1 and Run 4 repeat 2.

3.1 Fan gradient

Fan gradient is a useful metric for fan morphology. These data are shown in Figure 6: panel (a) shows an example of the raw data for a single run (Run 4), while (b) shows how the median fan gradient varied across the four runs. The decaying hydrographs of Runs 3 and 4 generated fans with the lowest gradients. In Run 2 (with flat hydrographs of the same volume as Runs 3 and 4), fan gradient was steepest. In Run 1 (when the flow variation of Runs 2–4 was replaced by the constant mean flow), fan gradient was intermediate between the two previous cases. t-tests suggest that median gradients for most runs were significantly different, except for the comparison between Runs 1-2 and Runs 3-4; see the Supporting Information for further detail on the t-tests (Table S3) and some problems with the assumption of independence for the fan slope data.

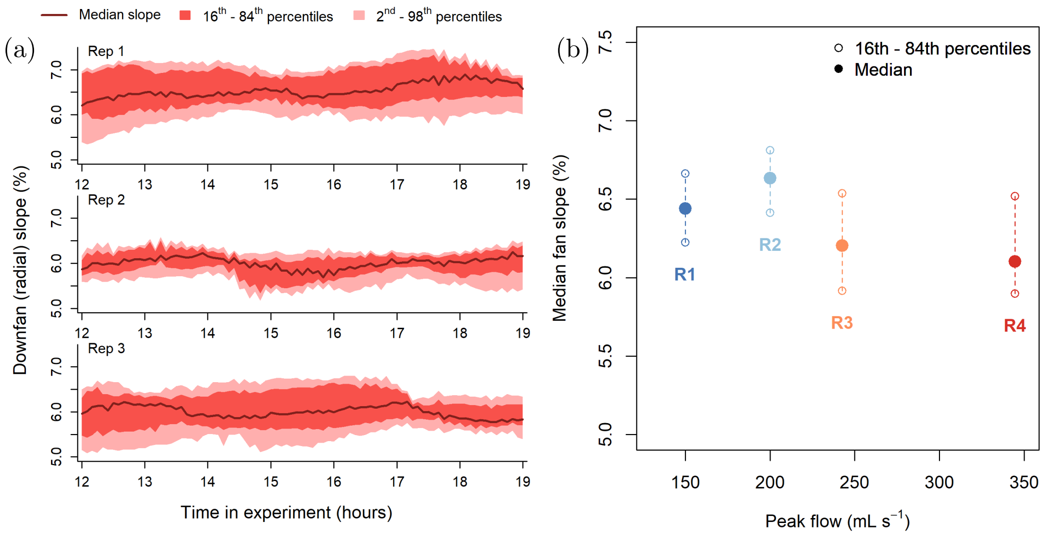

Figure 6. **(a)** Fan gradient variance in Run 4, from 88 downfan profiles for each minute. The three subplots show data for each repeat. **(b)** The distribution of median fan slope, from the population of median fan slopes across all repeats (i.e. data in R4 distribution taken from median lines in (a)). Data were sampled from 12–19 hours across all experimental repeats. Median fan slope was steeper for Run 2 than Run 1, but less steep for Runs 3 and 4.

3.2 Lateral (planform) change

The different hydrographs also influenced lateral channel mobility; we explored this effect by comparing successive flow maps. This change detection allowed us to quantify F_n, the percentage of the fan newly inundated each minute (Equation 1). F_n is a proxy for the lateral migration rate; high values of F_n (for instance, $F_n > 10\%$) can represent flow pattern ‘divergence’ (i.e. a rapid increase in the area occupied by flow). If a large area is simultaneously abandoned by the flow (high F_a), high values of F_n can also represent avulsion. However, we do not define these channel reorganization events quantitatively here (as in Leenman and Eaton (2021)). In this paper we are less concerned with discrete reorganization events, focusing instead on the quasi-continuous channel migration captured in the sequence of flow maps.

Figure 7 shows the temporal changes in F_n and F_a: panel (a) gives an example of raw data from Run 4 repeat 2, while panel (b) superimposes all high-to-low flow cycles for each run to demonstrate the general patterns in F_n. For comparison, panel (c) shows F_a, the rate of channel abandonment; this process is another important component of lateral mobility. However, the area newly inundated poses the greater hazard on natural fans, so we focus on F_n as our main metric for lateral channel mobility in the subsequent analysis. For reference, panel (d) shows the hydrographs for each experiment.

Lateral mobility (as measured by F_n) rose rapidly at the beginning of each flood event; as the peak flow increased from Run 2–4, so did the peak F_n value (Figure 7b). Given that high values of F_n can represent channel pattern divergence, this increase in the F_n maximum across Runs 2–4 suggests that any divergence events became larger as the peak flow increased. After the initial peak, F_n decreased throughout the flood hydrographs. F_n was at a minimum in the first minute of the low-flow period, when flow had reduced rapidly and was underfit for the channel formed by the preceding flood. The channel pattern then adjusted to the lower flow through slower lateral migration, with low rates of both F_n and F_a.

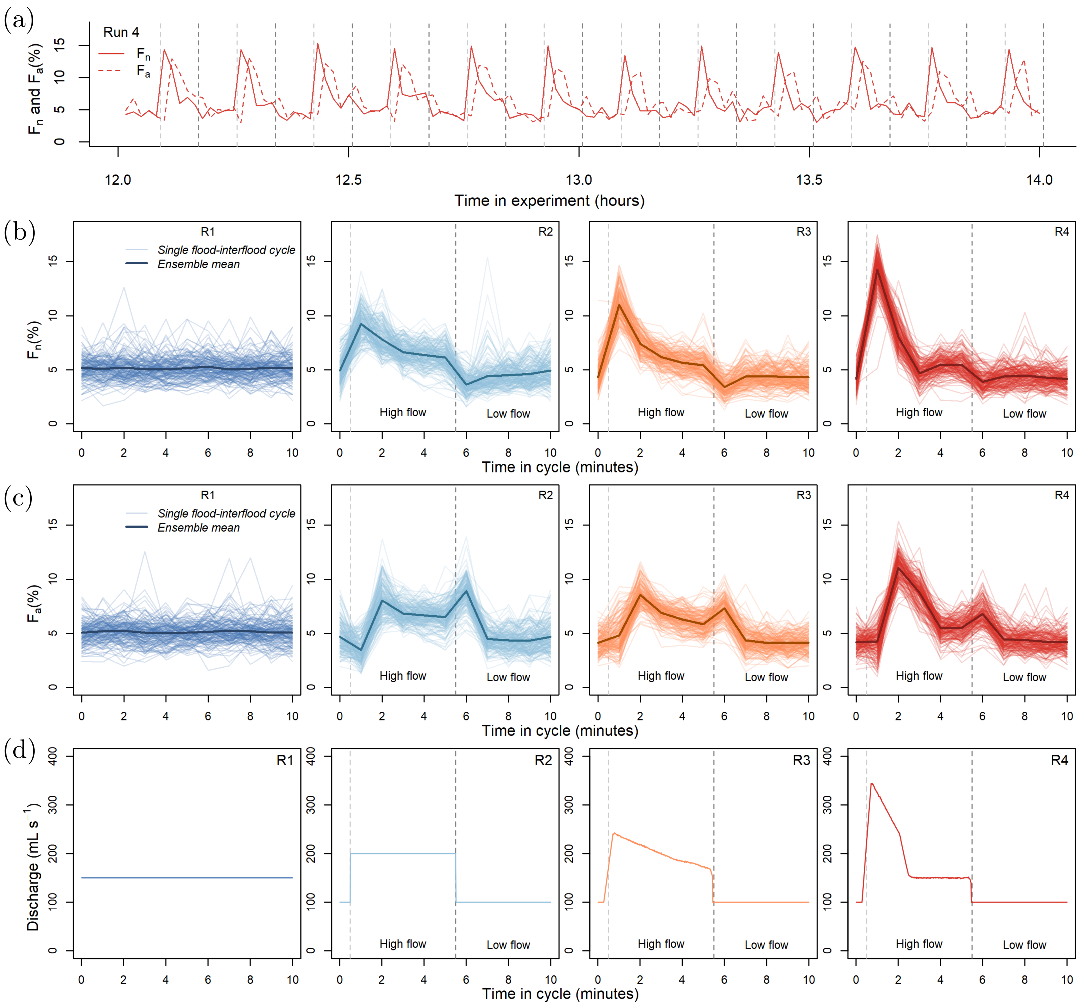

Figure 7. Temporal change in F_n, the percentage of the fan newly inundated each minute, and F_a, the percentage newly abandoned by flow. **(a)** An example of the change in F_n and F_a during Run 4 repeat 2 (over 12 10-minute flow cycles). The pale gray dashed lines mark the onset of high-flow periods (flood events), while the dark gray dashed lines mark the onset of low-flow periods. **(b-c)** Each cycle is overlaid, to show the general patterns of F_n (b) and F_a (c) during the 10-minute high-to-low flow cycle. **(d)** The corresponding hydrograph in each experiment (data from Figure 2).

In runs with floods, channel abandonment (F_a) peaked twice in the high-to-low flow cycle (Figure 7c). The first peak, in the second minute of the flood, can be attributed to both channel migration and flow rate. In Run 2, when flood flow was constant, the peak in F_a must reflect rapid channel adjustment following the peak in F_n (new inundation) in the previous minute. In Runs 3 and 4, this first F_a peak likely reflects the additional effect of the decaying flow rate, particularly in Run 4 when the decay is most rapid. The second peak, in the first minute of the low-flow period, can be attributed to this flow rate effect, and corresponds to a decrease in F_n with the same trigger.

The F_n patterns in Figure 7b are similar to the hydrograph shapes (7d). We therefore explored the relation between F_n and the flow in Figure 8. This figure shows that, as the maximum flow per minute (a proxy for the instantaneous flow) increased, F_n increased faster than linearly. For each experiment, the maximum F_n appears to be set by the peak flow, and the fastest reduction in F_n with flow rate is between the maximum and second-largest flow measurement; this effect becomes even more clear when flow rates for Runs 3 and 4 are normalized by the maximum flow in each experiment (Figure 7b). The rapid decay in mobility with flow rate indicates that flood events had their largest impact on inundation and planform channel change in the first minute of the flood.

The non-linear relation between the flow and F_n in Figure 8 suggests that the temporal distribution of water in a hydrograph governs the type of channel response to the flood event. If a flood of a given volume is delivered as a flatter, sustained hydrograph (as in Run 2), the potential avulsion or divergence at the start of that flood peak may be smaller, but lateral migration rates throughout the tail of the flood may be higher than in a flood in which the same volume of water is released as a larger peak that decays more rapidly.

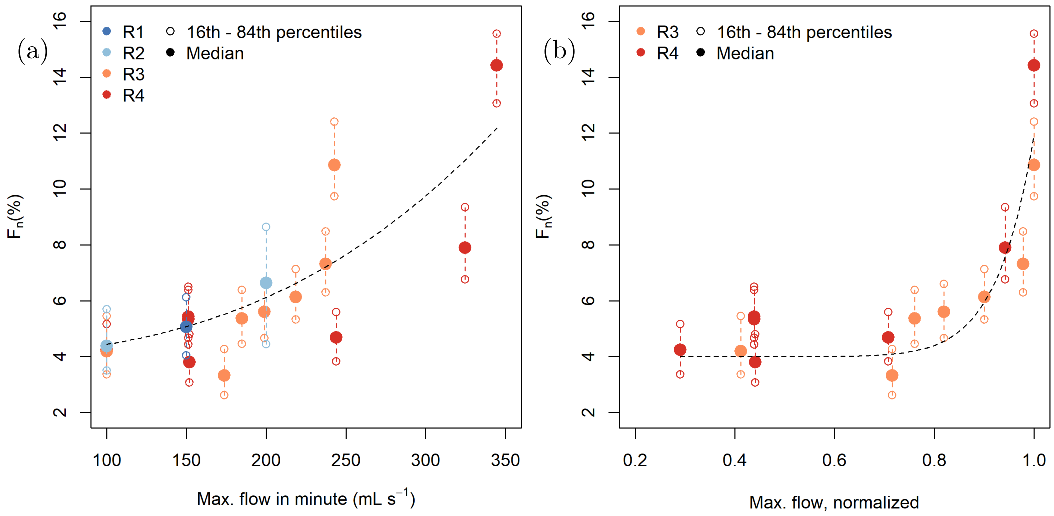

Figure 8. **(a)** The relationship between F_n, the percentage of the surface newly inundated, and the maximum flow in a given minute. The black dashed line marks a power-law fitted to the raw data underlying the distributions shown here; it has the form $y = a(x - x_0)^b + 4$, where $a = 5.2 \times 10^{-7}$, $b = 2.8$ and $x_0 = -33$ (2 s.f.). See Table S4 (SI) for information on the model fit. **(b)** Data from **(a)** re-plotted with the maximum flow in a minute normalized by the maximum flow in that experiment; only Runs 3 and 4 (with a wide range of flows) are shown. The black dashed line marks a power-law with the form $y = a(x)^b + 4$, where $a = 7.9$ and $b = 13$ (2 s.f.). See Table S5 (SI) for information on the model fit.

3.3 Geomorphic (vertical) change

Given the strong link between flow rates and lateral mobility (Figure 8), we also examined the relation between flow and vertically measured geomorphic change. The DoDs allowed us to quantify geomorphic change (M) as the sum of absolute erosion and deposition volumes in each minute (Equation 3). Figure 9 demonstrates how M varied over the 10-minute high-to-low flow cycle: panel (a) shows raw data from Run 4 repeat 2, while panel (b) superimposes all high-to-low flow cycles for each run to demonstrate the general temporal patterns in geomorphic change. The characteristic hydrographs for each run are included in panel (c).

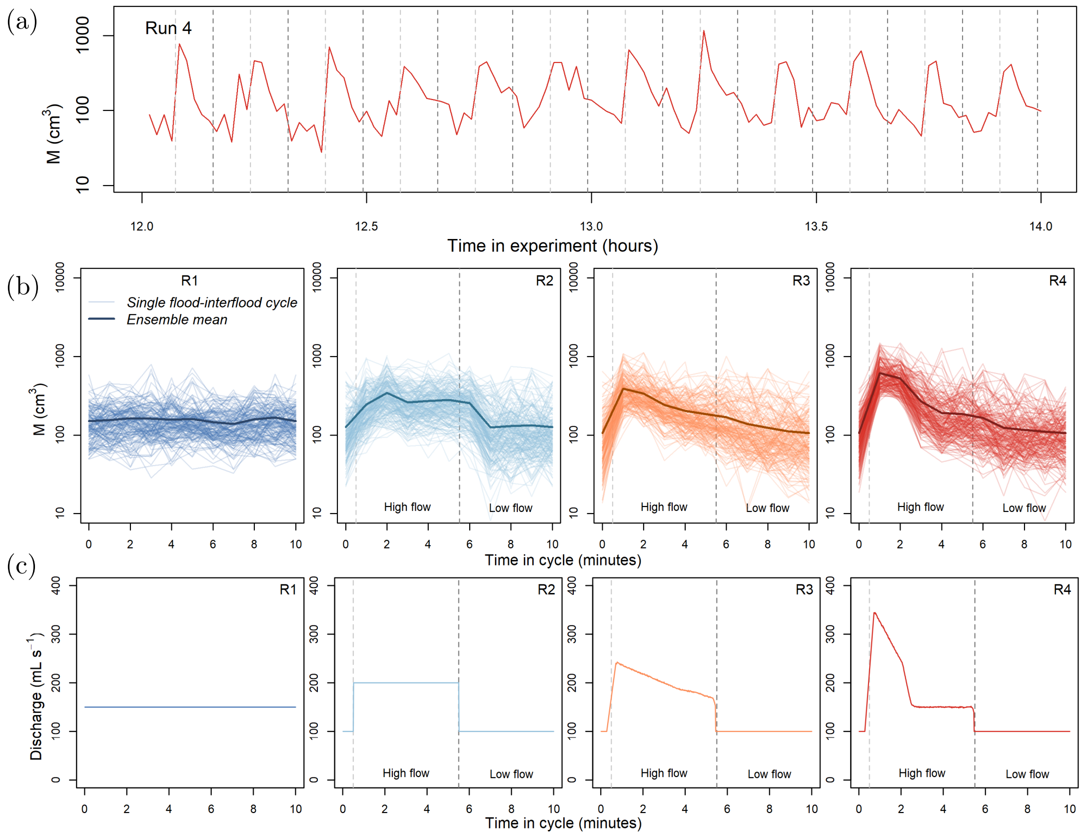

Figure 9. Temporal patterns in minute-to-minute geomorphic change (M). Note the y-axis log scale. **(a):** Sample data from Run 4 rep 2, showing geomorphic change over 12 10-minute flow cycles. **(b)** All cycles are superimposed, to show the general trend in geomorphic change during the high-to-low flow cycle. The bold line shows the mean of all cycles. **(c)** The corresponding hydrograph in each experiment (data from Figure 2).

As with F_n, the flood hydrograph shape again controlled the temporal pattern of geomorphic change (Figure 9). Generally, geomorphic change peaked with the flood peak, as a wave of new material was transported to the fan-head from the feeder channel. Geomorphic change was also high in the second minute of each high-flow period, due to reworking and onward transport of this 'new' sediment brought onto the fan in the preceding minute. In Run 2, reworking in the second minute even raised M to the maximum for that experiment. Raw erosion and deposition volumes are shown in Figure S4 (SI).

We summed M over each 10-minute high-to-low flow cycle to produce M_{C10}, shown in Figure 10. This figure implies that increasing the flood peak flow also increased the cumulative morphologic change across the whole 10-minute high-to-low flow cycle; M_{C10} was lowest for Run 1, with the lowest peak flow, and highest for Run 4. Most geomorphic change occurred during the flood events (Figure S5, SI). The exact nature of the relation between peak flow and M_{C10} is unclear; one repeat of Run 2 was very active, so that M_{C10} values for Runs 2 and 3 were not significantly different. Nevertheless, because erosion and deposition volumes provide minimum and maximum estimates (respectively) of sediment transport in our experiment, M_{C10} is a useful measure of the geomorphic activity induced by each hydrograph. Figure 10 therefore highlights how constant flow dampened geomorphic activity and variable flow enhanced it, even though the same water volume dispersed across the fan in each 10-minute flow cycle.

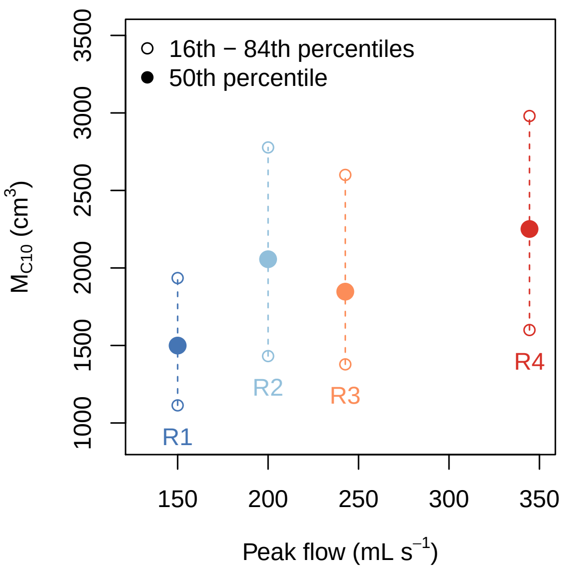

Figure 10. Cumulative geomorphic change over the 10-minute high-to-low flow cycle (M_{C10}). Cumulative change varied with hydrograph shape; it was smallest with constant flow (R1) and greatest with high flood peaks (R4). Runs 2 and 3 were not significantly different; see Table S6 (SI) for p-values.

To further investigate the influence of flow on geomorphic change, in Figure 11 we compared the maximum flow at each minute in the high-to-low flow cycle to M in that minute. The figure shows that across all experimental runs, as the flow increased, the associated geomorphic change volume increased faster than linearly. This non-linear relation indicates that the temporal distribution of water during a flood event is a crucial control on the volumes of material eroded, transported and deposited on the fan.

Finally, we examined the spatial distribution of geomorphic change using down-fan profiles extracted from five-minute DoDs that spanned either flood events or low-flow periods (Figure 12). Across all runs, geomorphic change was greatest at the fan-head. Figure 12 shows that during flood events, erosion dominated at the fan-head, while deposition was fairly evenly distributed down the fan with a low peak just below the fan-head. Conversely, the low-flow periods resulted in a zone of concentrated deposition at the fan-head, while erosion peaked slightly downstream. The magnitude of fan-head change increased as the flood peak increased from Run 2–4. As with the preceding figures, these

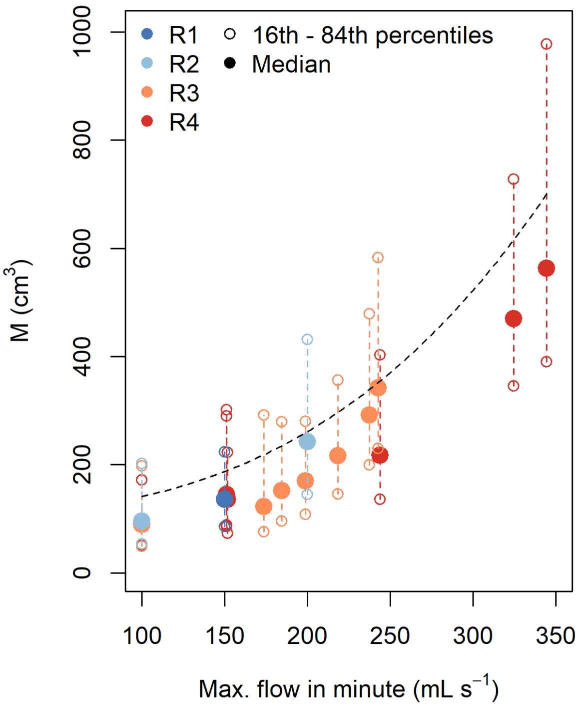

Figure 11. Relationship between the volume of geomorphic change (M) in a minute, and the maximum flow in a minute. The black dashed line marks a power-law fitted to the raw data underlying the distributions shown here; it has the form $y = a(x - x_0)^b + 100$, where $a = 1.2 \times 10^{-6}$, $b = 3.3$ and $x_0 = -94$ (2 s.f.). Most distributions of M were positively-skewed, causing the relation to plot higher than the medians. See Table S8 (SI) for information on model fit.

data highlight how the geomorphic activity on the fan intensified as the flood peak flow increased, even though the same water volume dispersed across the fan in all flood events.

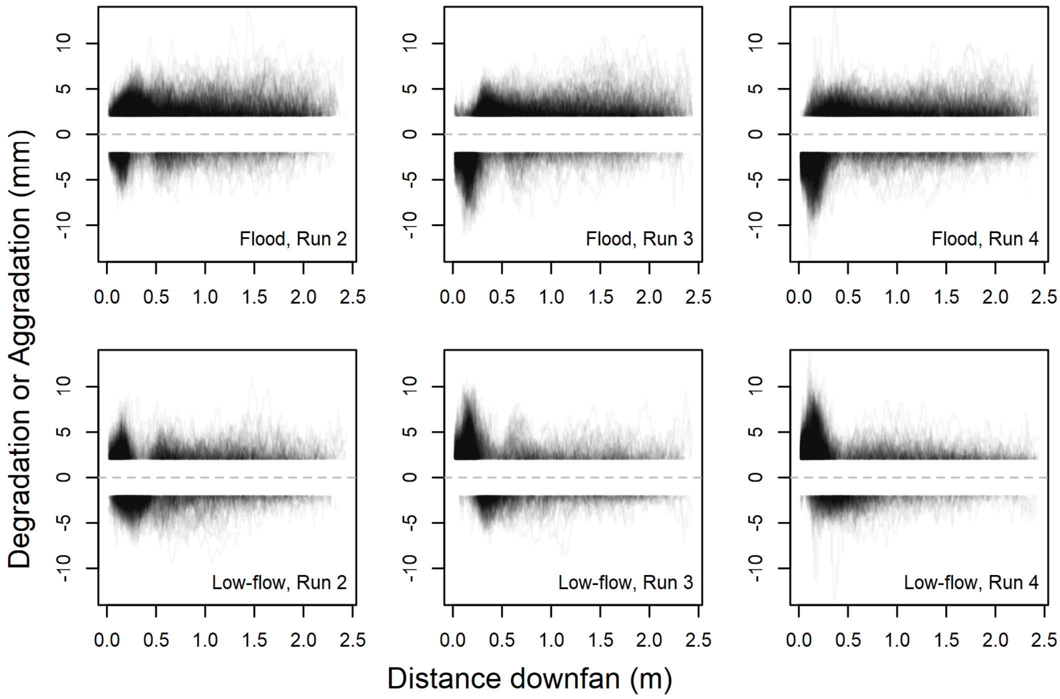

Figure 12. The downfan pattern of deposition and erosion, during floods (above) and low-flow periods (below). Seven equally-spaced downfan profiles were extracted from the five-minute DoD spanning each flood event or low-flow period. Geomorphic change of < 2 mm was discarded.

4 Discussion

4.1 Key findings and unresolved questions

Our experiments exhibited a distinct non-linear relation between the flow rate and our two measures of geomorphic activity: F_n (a proxy for lateral mobility), and M (summing vertically measured geomorphic change). As the flow increased, F_n and M increased faster than linearly (Figures 8 and 11). This non-linearity explains key differences between our experiments, and particularly the increase in cumulative geomorphic change (M_{C10}) as peak flow increased from Run 1 to Run 4 (Figure 10). Although the exact nature of the relation in Figure 10 is unclear, the non-linear influence of flow on M explains why the addition of flood events caused Runs 2–4 to be more geomorphically active, and in particular why Run 4, that with the highest peak flow, was most active.

Many bedload transport formulae predict sediment transport as a non-linear function of some flow metric (Barry et al., 2004; DuBoys, 1879; Meyer-Peter & Müller, 1948; Parker, 1990; Shields, 1936; Schoklitsch, 1962; Wilcock & Kenworthy, 2002; Wilcock & Crowe, 2003; Wong & Parker, 2006). Eaton et al. (2020) further showed that sediment transport scales with the volume of erosion in laterally active streams. It is perhaps unsurprising then, that we observed a non-linear relation between flow rates and volumes of geomorphic change. We infer that the non-linear dependence of sediment transport on flow causes this non-linearity in our data. That is, when flow rises, erosion and sediment transport rise faster-than-linearly; because the fan is a closed system, deposition rises with transport, thereby causing M to scale non-linearly with flow.

The sensitivity of F_n and M at high flows may also reflect the crossing of stability thresholds set by coarse grains. Experiments in a laterally mobile stream by Eaton et al. (2020) showed that as flow increased and as much as 80% of the bed material was mobilized, it was only once flows were great enough to mobilize the largest grains present that channel dimensions were modified. Consequently, they postulated that overall channel stability reflects the stability of a small population of immobile or partially mobile large grains. In a previous study analyzing what we present here as Run 1 in more detail, we also observed that in-channel deposition around accumulations of the largest grains disrupted autogenic flow pattern cycling (Leenman & Eaton, 2021). The non-linear relation between geomorphic change and flow in our data may therefore indicate that channel dimensions are regulated by the (im)mobility of the coarsest grains on the fan.

Observations from this study illuminate the role that flow variability plays in controlling fan geometry, and fan gradient in particular. Different 'types' of flow variability generated different fan gradients (Figure 6): the 'flat' hydrographs in Run 2 generated steeper fans than those built by constant flow, while the 'peaked' hydrographs in Runs 3 and 4 generated the lowest fan gradients. It is difficult to interpret this pattern without accurate water-depth data with which to determine the shear stress distribution across the fan, and therefore the conditions driving entrainment and deposition. Nevertheless, Figure 12 can be used to provide insight as to whether it is flood events, or the periods of low flow between them, that set the fan gradient.

Comparing between low-flow and flood periods, data from our experiments suggest that flow magnitude may exert an important influence on the location of geomorphic change, and through that, the gradient of a fan. During low-flow periods in Runs 2–4, sediment transport onto the fan slowed at the fan-head, creating a deposition zone that steepened the fan (Figure 12). Conversely, flood events eroded the fan-head and caused deposition on the lower fan which ultimately decreased fan gradient. Hooke (1968b) observed that the flow magnitude controlled the downfan location of erosion and deposition in a similar way, in an experiment with variable discharge. In our experiments, the steepening or shallowing of fan gradient that resulted from the spatial distribution of deposition is weakly evident in Figure S7 (SI), which shows how fan gradient adjusted throughout the 10-minute high-to-low flow cycle.

Based on the figures discussed above, we speculate that the steeper gradient in Run 2 results from the relatively low peak flow of that experiment, which prevented floods from eroding the fan-head sufficiently to counterbalance the steepening in the low-flow periods (which had equal magnitude across Runs 2–4). Conversely, it seems that the peak flows in Runs 3 and 4 were high enough to erode the fan-head and redistribute sediment to the lower fan, generating low gradients. Theory, experiments and field data indicate that the slope of alluvial fans and unconfined channels decreases with increasing discharge or basin area (a proxy for discharge) (Blair & McPherson, 1994a; Bull, 1962; Delorme et al., 2018; Harvey et al., 1999; Métivier et al., 2017; Seizilles et al., 2013; Silva et al., 1992; Whipple et al., 1998). Our experimental data extend this observation, suggesting that for the same average discharge, fan slope decreases as maximum flood magnitude increases when flood pulses are present. However, this suggestion remains speculative; additional experiments with a wider range of hydrograph shapes, and data on the down-fan distribution of shear stress, are necessary to further evaluate this hypothesis. Nevertheless, the different gradients generated by our different hydrographs demonstrate a need to incorporate multiple types of variability when modeling stream geomorphology.

A relatively narrow range of gradients was attained across the four experiments, which may reflect the short five-minute durations of the floods we imposed. Theory suggests that for a perturbation to fully regrade a geomorphic system, the perturbation must continue for longer than the time required to regrade the system (the 'equilibrium' timescale) (Paola et al., 1992; Straub et al., 2020). Perturbations shorter than the equilibrium timescale are not expected to drive the system to a new topographic steady state. In our data, the weak effect of individual flood events on fan gradient is highlighted by the comparison of Figures 6 and S7 (SI). Figure S7 shows that each five-minute flood event had a minute influence on fan gradient. However, over many repeated flood events, the characteristic hydrographs in Runs 2-4 began to influence fan gradient in distinctive ways, through the accumulated effects of multiple perturbations (Figure 6). Further experiments with longer duration perturbations could affect fan gradient in different ways (e.g. Chapter 6 in Leenman (2021)).

The different hydrographs employed in our experiments raise the question of whether flood peak magnitude or duration has a stronger control on flood response. Field evidence offered by Costa and O'Connor (1995) and Huckleberry (1994) suggests that flood duration is more important than flood magnitude. These authors expected a long, moderately sized flood to be more geomorphically effective than a short, large-magnitude flood. Figure 10, which compares the peak flow in our four experiments to cumulative (summed) geomorphic change, can be used to investigate this question; however, one can interpret Figure 10 to either counter or support their field observations. On one hand, Figure 10 suggests that cumulative geomorphic change scales with flood peak magnitude, an observation that contrasts the field data. Alternatively, Figure 10 could provide some support for those authors' inferences, given that Run 2 had lower, longer 'peak' flows than Run 3, but generated larger M_{C10} values (at least on average). However, this second interpretation is weakened by the lack of a significant difference between Runs 2 and 3 in Figure 10, and by high M_{C10} values for Run 4. Further experiments with a wider range of flood durations could shed more light on the competing effects of flood magnitude and duration.

The survey frequency in our experiment was high relative to the flood durations, which introduces some challenges in comparing our results to field studies. In the field, one can hope to capture DEMs before and after a flood; these data only allow calculation of *net* topographic change. It is rare to obtain topographic data at regular intervals throughout a flood event as we have here, allowing to estimate the *cumulative* geomorphic change. While the cumulative geomorphic change (M_{C10}) generally scaled with the peak flow in our experiments (Figure 10), the net geomorphic change was similar across all experiments (Figure S6, SI). This difference has two probable causes. Firstly, 'topographic compensation' (Lindsay & Ashmore, 2002) between DEMs means that a DoD between the first and last DEM in a 10-minute flow cycle (used to calculate net change) fails to capture local cutting and filling at shorter time-frames. Conversely, these processes are captured in the one-minute DoDs that we summed to calculate M_{C10}. Secondly, a key difference between our hydrographs was that they generated different spatial distributions of deposition (Figure 12). However, these spatial patterns are not captured in M volumes. We therefore emphasize that it is necessary to compare both volumes and spatial patterns of geomorphic change to understand the geomorphic impacts of different hydrographs.

While we varied the flow in Runs 2-4, the sediment feed rate was constant in all experiments. The sediment concentration therefore varied; it was 1.8% by volume during Run 1, and during Run 4 (with the largest flow variations), concentration varied from 0.8% to 2.8%. Sediment and water were input to the 0.5 m-long feeder channel, which buffered the effect of these variations; the feeder channel aggraded when the sediment supply exceeded transport capacity, and was scoured to increase the sediment concentration during high flows. This cyclic aggradation and degradation upstream of the fan-head dampened the effect of sediment concentration variability.

Nevertheless, variable sediment concentration can aid in interpreting some of our results. In particular, low-flows featured fan-head deposition (Figure 12) and ensuing steepening (Figure S7); these results may reflect the higher sediment concentration during low flows. The fan-head deposition observed may also reflect downstream propagation of the feeder-channel aggradation. Conversely, fan-head erosion during high-flows may reflect a lower sediment concentration, and the downstream propagation of feeder-channel erosion. In comparison to fan gradient, our metrics for planform change (F_n) and geomorphic change (M) are less affected by sediment concentration; these are spatially averaged measures that represent the dynamics of the fan as a whole, so that aggradation and degradation at the fan-head play a lesser role.

4.2 Implications for natural fans and their representation in models

In our experiments, variable and constant flow produced different fan morphology, lateral mobility, and geomorphic change rates, despite an equal mean flow across all experiments. Our results add to a growing body of evidence that variable flows play a non-negligible role in fan and fan-delta dynamics (Barefoot et al., 2021; Ganti et al., 2016; Piliouras et al., 2017; Miller et al., 2019). Using the mean flow as a constant flow (Run 1) dampened geomorphic activity and generated fans with different gradients (Figures 7, 9, and 6, respectively). These results indicate that the mean flow alone is not a suitable predictor of fan gradient nor lateral and vertical (i.e. geomorphic) change.

Our experimental design demonstrates the distortions introduced through different scales of temporal averaging in the flow to fans. When we compare a temporally varying flood event (i.e. Run 3 or 4) with a constant-flow flood (i.e. Run 2), the latter produced steeper fans with lower maxima in lateral mobility and geomorphic change. Moreover, when we compare our variable flow experiments (Runs 2–4) to a constant mean flow (Run 1), fan gradient was again different, and geomorphic activity was further dampened. As such, our data show that averaging out the variability in a hydrological series, across a series of flood events or even within a hydrograph, can under-represent the range of geomorphic activity that would result from those flow variations, particularly given the non-linear relations between flow and geomorphic activity.

Based on our findings, we question whether it is appropriate to use a single constant flow to represent the range of flows on natural fans. While this approach has been taken in most alluvial fan experiments that we are aware of, our results show that constant and varied flow produce different fan morphology and dynamics when the mean flow is equal. Therefore, the mean flow was not a suitable 'representative discharge' for our experimental fans—neither for replicating fan gradient, nor for lateral mobility and sediment movement volumes.

Hooke and Rohrer (1979) attempted to determine a representative discharge on alluvial fans. Rather than the bankfull flood, they defined the representative discharge as the single constant flow that built fans with a gradient equal to that of fans built with a range of flows. Their experiments indicated that the representative discharge was somewhere between the 64th and 75th percentile of flows. However, even if one can use a 'representative' constant flow to recreate fan gradient, our data showed that the geomorphic mechanisms by which this gradient is achieved is not the same in both cases. If instead of the mean flow, we had used a constant flow equal to the 70th percentile of our variable flows (following Hooke and Rohrer (1979)), Figures 9-11 suggest that we would likely have built fans with lower maximum and cumulative reworking rates than in our widely-varying flow experiments. Thus, even if the two experiments converged on similar fan gradients, in the constant flow experiment we would still fail to represent the range of geomorphic change and lateral mobility rates, and therefore, the hazard regime, on a fan subject to variable flows. We thus propose that it is generally not appropriate to employ a single representative flow in alluvial fan studies, unless the research question or hazard management problem at hand is focused only on a single response variable such as the fan gradient.

5 Conclusion

We conducted four alluvial fan experiments to examine the role that flow variability plays in fan morphodynamics. We compared one experiment with constant flow to three with temporally varying flow, each with a series of repeated flood hydrographs: one experiment had flat hydrographs, one had moderate flood peaks that decayed slowly, and one had higher flood peaks that decayed rapidly. Mean flow and sediment supply were equal across all experiments. The four experiments generated different fan gradients, lateral mobility rates and geomorphic change (erosion and deposition): greater geomorphic change and lower gradients were associated with greater flood peaks. Moreover, the type of flow variability was important: flat and decaying hydrographs with the same total flood volume had different effects. Fans subject to flat hydrographs with a lower-magnitude peak were steeper, but the maximum lateral mobility and geomorphic change rates attained were lower. Conversely, fans subject to higher-magnitude flood peaks that decayed rapidly were less steep, but attained higher maximum activity rates.

The instantaneous flow rate was a key control on lateral mobility and geomorphic change. The maximum flow in a given minute (a proxy for the instantaneous flow) was related non-linearly to lateral channel mobility and the geomorphic change rate; both increased faster than linearly as the flow increased. This non-linearity meant that as the peak flow increased across our three hydrograph shapes, lateral mobility and geomorphic change achieved considerably higher maxima.

These results demonstrate that temporally averaged flow metrics, such as the mean flow, mean flood flow or total flood volume, are not suitable predictors of fan morphology (i.e. gradient) or flood impacts. Applying such metrics to our results would lead us to underestimate the maximum lateral mobility and geomorphic change rates, or to wrongly predict fan gradient. We therefore question the use of a 'representative' flow in alluvial fan experiments and simulations. The choice of a representative flow, when one must be used, will depend on the aspect of fan morphology or dynamics that is of interest.

Finally, our experiments shed light on how changes to flood hydrograph shape on natural fans could influence fan responses to flood events. For a rainfall event of a given intensity and duration, the associated flood hydrograph shape may change in response to land cover change or flow regulation. By modeling fan responses to different flood hydrographs, we advance understanding of how hydrograph shape can impact streams on alluvial fans and their responses to flood events.

Acknowledgments

A. Leenman was funded by a UBC Four-Year Fellowship. Experimental construction was funded through an NSERC Discovery Grant to B. Eaton. Thanks to Mike Church and Lauren Vincent for helpful comments and discussions which greatly improved the quality and clarity of our manuscript. We would also like to thank Kimberley Litwin Miller, Anastasia Piliouras and one anonymous reviewer for thorough and insightful reviews.

The data underlying all figures in this manuscript are available from the Canadian Federated Research Data Repository (FRDR) at https://doi.org/10.20383/102.0482.

References

Agisoft photoscan professional. (2018, Dec). (Structure-from-Motion photogrammetry software, accessed via https://www.agisoft.com/downloads/installer/)

Ashworth, P. J., Best, J. L., Leddy, J. O., & Geehan, G. W. (1994). The physical modelling of braided rivers and deposition of fine-grained sediment. In M. J. Kirkby (Ed.), *Process models and theoretical geomorphology* (pp. 115–139). John Wiley and Sons.

Barefoot, E. A., Nittrouer, J. A., & Straub, K. M. (2021). Non-monotonic floodplain responses to changes in flooding intensity. *Journal of Geophysical Research: Earth Surface*, *126*(10), e2021JF006310. doi: https://doi.org/10.1029/2021JF006310

Barry, J. J., Buffington, J. M., & King, J. G. (2004). A general power equation for predicting bed load transport rates in gravel bed rivers. *Water Resources Research*, *40*(10). doi: https://doi.org/10.1029/2004WR003190

Beaumont, P., & Oberlander, T. (1971). Observations on stream discharge and competence at Mosaic Canyon, Death Valley, California. *Geological Society of America Bulletin*, *82*(6), 1695-1698.

Blair, T. C., & McPherson, J. G. (1994a). Alluvial fan processes and forms. In *Geomorphology of desert environments* (pp. 354–402). Springer.

Blair, T. C., & McPherson, J. G. (1994b). Alluvial fans and their natural distinction from rivers based on morphology, hydraulic processes, sedimentary processes, and facies assemblages. *Journal of sedimentary research*, *64*(3a), 450–489.

Bryant, M., Falk, P., & Paola, C. (1995). Experimental study of avulsion frequency and rate of deposition. *Geology*, *23*(4), 365-368. doi: 10.1130/0091-7613(1995)023<0365:ESOAFA>2.3.CO

Bull, W. B. (1962). Relations of alluvial fan size and slope to drainage basin size and lithology in western Fresno County, California. *US Geological Survey Professional Paper*, *450*, 51–53.

Church, M., & Ferguson, R. (2015). Morphodynamics: Rivers beyond steady state. *Water Resources Research*, *51*(4), 1883–1897.

Church, M., & Jakob, M. (2020). What is a debris flood? *Water resources research*, *56*(8), e2020WR027144.

Clarke, L., Quine, T. A., & Nicholas, A. (2010). An experimental investigation of autogenic behaviour during alluvial fan evolution. *Geomorphology*, *115*(3), 278-285.

Costa, J. E., & O'Connor, J. E. (1995). Geomorphically effective floods. In J. Costa, A. Miller, K. Potter, & P. Wilcock (Eds.), *Natural and anthropogenic influences in fluvial geomorphology* (p. 45-56). American Geophysical Union (AGU) Monograph 89. doi: https://doi.org/10.1029/GM089p0045

Davidson, S. K., Hartley, A. J., Weissmann, G. S., Nichols, G. J., & Scuderi, L. A. (2013). Geomorphic elements on modern distributive fluvial systems. *Geomorphology*, *180-181*, 82 - 95. doi: https://doi.org/10.1016/j.geomorph.2012.09.008

Davidson, S. L., & Eaton, B. C. (2018). Beyond regime: A stochastic model of floods, bank erosion, and channel migration. *Water Resources Research*, *54*(9), 6282–6298.

Davies, T. R., & Korup, O. (2007). Persistent alluvial fanhead trenching resulting from large, infrequent sediment inputs. *Earth Surface Processes and Landforms*, *32*(5), 725–742.

Davies, T. R., McSaveney, M. J., & Clarkson, P. J. (2003). Anthropic aggradation of the Waiho River, Westland, New Zealand: microscale modelling. *Earth Surface Processes and Landforms*, *28*(2), 209–218.

De Haas, T., Kruijt, A., & Densmore, A. (2018). Effects of debris-flow magnitude–frequency distribution on avulsions and fan development. *Earth Surface Pro-*

cesses and Landforms, *43*(13), 2779–2793.

De Haas, T., Van Den Berg, W., Braat, L., & Kleinhans, M. G. (2016). Autogenic avulsion, channelization and backfilling dynamics of debris-flow fans. *Sedimentology*, *63*(6), 1596–1619.

Delorme, P., Devauchelle, O., Barrier, L., & Métivier, F. (2018). Growth and shape of a laboratory alluvial fan. *Physical Review E*, *98*(1), 012907.

Delorme, P., Voller, V., Paola, C., Devauchelle, O., Lajeunesse, É., Barrier, L., & Métivier, F. (2017). Self-similar growth of a bimodal laboratory fan. *Earth Surface Dynamics*, *5*(2), 239 - 252. doi: 10.5194/esurf-5-239-2017

DuBoys, M. (1879). Etudes du regime et l'action exercée par les eaux sur un lit a fond de graviers indefinement affouilable. *Annals des Ponts et Chaussées*, *5*, 141–195.

Eaton, B. C. (2013). Hydraulic Geometry: Empirical Investigations and Theoretical Approaches. In E. W. John F. Shroder (Ed.), *Treatise on geomorphology* (Vol. 9 (Fluvial Geomorphology), p. 313-329). San Diego: Academic Press. doi: https://doi.org/10.1016/B978-0-12-374739-6.00243-8

Eaton, B. C., MacKenzie, L. G., & Booker, W. H. (2020). Channel stability in steep gravel–cobble streams is controlled by the coarse tail of the bed material distribution. *Earth Surface Processes and Landforms*, *45*(14), 3639-3652. doi: https://doi.org/10.1002/esp.4994

Field, J. (2001). Channel avulsion on alluvial fans in southern Arizona. *Geomorphology*, *37*(1-2), 93-104.

Ganti, V., Chadwick, A. J., Hassenruck-Gudipati, H. J., Fuller, B. M., & Lamb, M. P. (2016). Experimental river delta size set by multiple floods and backwater hydrodynamics. *Science advances*, *2*(5), e1501768.

Guerit, L., Métivier, F., Devauchelle, O., Lajeunesse, É., & Barrier, L. (2014). Laboratory alluvial fans in one dimension. *Physical Review E*, *90*(2), 022203.

Gutiérrez, F., Gutiérrez, M., & Sancho, C. (1998). Geomorphological and sedimentological analysis of a catastrophic flash flood in the Arás drainage basin (Central Pyrenees, Spain). *Geomorphology*, *22*(3-4), 265–283.

Hamilton, P. B., Strom, K., & Hoyal, D. C. (2013). Autogenic incision-backfilling cycles and lobe formation during the growth of alluvial fans with supercritical distributaries. *Sedimentology*, *60*(6), 1498-1525.

Harvey, A. M., Silva, P. G., Mather, A. E., Goy, J. L., Stokes, M., & Zazo, C. (1999). The impact of Quaternary sea-level and climatic change on coastal alluvial fans in the Cabo de Gata ranges, southeast Spain. *Geomorphology*, *28*(1), 1-22. doi: https://doi.org/10.1016/S0169-555X(98)00100-7

Hijmans, R. J. (2020). raster: Geographic data analysis and modeling [Computer software manual]. Retrieved from `https://CRAN.R-project.org/package=raster` (R package version 3.4-5)

Hooke, R. L. (1967). Processes on arid-region alluvial fans. *The Journal of Geology*, *75*(4), 438–460.

Hooke, R. L. (1968a). Model geology: prototype and laboratory streams: discussion. *Geological Society of America Bulletin*, *79*(3), 391–394.

Hooke, R. L. (1968b). Steady-state relationships on arid-region alluvial fans in closed basins. *American Journal of Science*, *266*(8), 609–629.

Hooke, R. L., & Rohrer, W. L. (1979). Geometry of alluvial fans: Effect of discharge and sediment size. *Earth Surface Processes*, *4*(2), 147-166. doi: 10.1002/esp.3290040205

Huckleberry, G. (1994, 12). Contrasting channel response to floods on the middle Gila River, Arizona. *Geology*, *22*(12), 1083-1086. doi: 10.1130/0091-7613(1994)022<1083:CCRTFO>2.3.CO;2

Jakob, M., Clague, J. J., & Church, M. (2016). Rare and dangerous: Recognizing extra-ordinary events in stream channels. *Canadian Water Resources Journal/Revue canadienne des ressources hydriques*, *41*(1-2), 161–173.

Jakob, M., Weatherly, H., Bale, S., Perkins, A., & MacDonald, B. (2017). A Multi-Faceted Debris-Flood Hazard Assessment for Cougar Creek, Alberta, Canada. *Hydrology*, *4*(1), 7.

Kassambara, A. (2020). rstatix: Pipe-friendly framework for basic statistical tests [Computer software manual]. Retrieved from `https://CRAN.R-project.org/package=rstatix` (R package version 0.5.0)

Kesel, R. H., & Lowe, D. R. (1987). Geomorphology and sedimentology of the Toro Amarillo alluvial fan in a humid tropical environment, Costa Rica. *Geografiska Annaler: Series A, Physical Geography*, *69*(1), 85–99.

Larsen, M. C., Wieczorek, G. F., Eaton, L., & Torres-Sierra, H. (2001). Natural hazards on alluvial fans: the debris flow and flash flood disaster of December 1999, Vargas state, Venezuela. In W. Sylva (Ed.), *Proceedings of the sixth caribbean islands water resources congress* (Vol. 965, pp. 1–7). Mayagüez, Puerto Rico.

Leenman, A. (2021). *Environmental variability and geomorphic responses on alluvial fans: An experimental study* (Unpublished doctoral dissertation). University of British Columbia, Vancouver, Canada.

Leenman, A., & Eaton, B. C. (2021). Mechanisms for avulsion on alluvial fans: insights from high-frequency topographic data. *Earth Surface Processes and Landforms*, *46*(6), 1111-1127. doi: 10.1002/esp.5059.

Lindsay, J. B., & Ashmore, P. E. (2002). The effects of survey frequency on estimates of scour and fill in a braided river model. *Earth Surface Processes and Landforms*, *27*(1), 27-43. doi: https://doi.org/10.1002/esp.282

Métivier, F., Lajeunesse, E., & Devauchelle, O. (2017). Laboratory rivers: Lacey's law, threshold theory, and channel stability. *Earth Surface Dynamics*, *5*(1), 187–198. Retrieved from `https://esurf.copernicus.org/articles/5/187/2017/` doi: 10.5194/esurf-5-187-2017

Meyer-Peter, E., & Müller, R. (1948). Formulas for bed-load transport. In *Iahsr 2nd meeting, stockholm, appendix 2.*

Miller, K. L., Kim, W., & McElroy, B. (2019). Laboratory Investigation on Effects of Flood Intermittency on Fan Delta Dynamics. *Journal of Geophysical Research: Earth Surface*, *124*(2), 383–399.

Paola, C., Heller, P. L., & Angevine, C. L. (1992). The large-scale dynamics of grain-size variation in alluvial basins, 1: Theory. *Basin research*, *4*(2), 73–90.

Paola, C., Straub, K., Mohrig, D., & Reinhardt, L. (2009). The "unreasonable effectiveness" of stratigraphic and geomorphic experiments. *Earth-Science Reviews*, *97*(1-4), 1–43.

Parker, G. (1979). Hydraulic geometry of active gravel rivers. *Journal of the Hydraulics Division*, *105*(9), 1185-1201. doi: 10.1061/JYCEAJ.0005275

Parker, G. (1990). Surface-based bedload transport relation for gravel rivers. *Journal of hydraulic research*, *28*(4), 417–436.

Peakall, J., Ashworth, P., & Best, J. (1996, January 1). Physical modelling in fluvial geomorphology: principles, applications and unresolved issues. In *The scientific nature of geomorphology: Proceedings of the 27th binghamton symposium in geomorphology* (pp. 221–253). John Wiley and Sons.

Pearthree, P. A., Klawon, J. E., & Lehman, T. W. (2004). *Geomorphology and hydrology of an alluvial fan flood on Tiger Wash, Maricopa and La Paz Counties, west-central Arizona* (Tech. Rep. No. 04-02). Arizona Geological Survey.

Piliouras, A., Kim, W., & Carlson, B. (2017). Balancing aggradation and progradation on a vegetated delta: The importance of fluctuating discharge in depositional systems. *Journal of Geophysical Research: Earth Surface*, *122*(10), 1882–1900.

R Core Team. (2021). R: A language and environment for statistical computing [Computer software manual]. Vienna, Austria. Retrieved from `https://www.R-project.org/`

Rahn, P. H. (1967). Sheetfloods, streamfloods, and the formation of pediments. *Annals of the Association of American Geographers*, *57*(3), 593-604.

Reitz, M. D., & Jerolmack, D. J. (2012). Experimental alluvial fan evolution: Channel dynamics, slope controls, and shoreline growth. *Journal of Geophysical Research: Earth Surface*, *117*(F2), F02021.

Reitz, M. D., Jerolmack, D. J., & Swenson, J. B. (2010). Flooding and flow path selection on alluvial fans and deltas. *Geophysical Research Letters*, *37*(6), L06401. doi: 10.1029/2009GL041985

Santo, A., Santangelo, N., Di Crescenzo, G., Scorpio, V., De Falco, M., & Chirico, G. B. (2015). Flash flood occurrence and magnitude assessment in an alluvial fan context: the October 2011 event in the Southern Apennines. *Natural Hazards*, *78*(1), 417–442.

Schlichting, H., & Gersten, K. (2016). *Boundary-layer theory.* Springer.

Schoklitsch, A. (1962). *Handbuch des wasserbaues* (3rd ed.). Vienna: Springer.

Schumm, S. A., Mosley, M. P., & Weaver, W. (1987). *Experimental fluvial geomorphology.* New York: John Wiley and Sons Inc.

Seizilles, G., Devauchelle, O., Lajeunesse, E., & Métivier, F. (2013, May). Width of laminar laboratory rivers. *Phys. Rev. E*, *87*, 052204. doi: 10.1103/PhysRevE.87.052204

Shields, A. (1936). *Anwendung der aehnlichkeitsmechanik und der turbulenzforschung auf die geschiebebewegung* (Unpublished doctoral dissertation). Technical University Berlin.

Silva, P., Harvey, A., Zazo, C., & Goy, J. (1992). Geomorphology, depositional style and morphometric relationships of Quaternary alluvial fans in the Guadalentin depression (Murcia, southeast Spain). *Zeitschrift für Geomorphologie*, *36*(3), 325–341.

Straub, K. M., Duller, R. A., Foreman, B. Z., & Hajek, E. A. (2020). Buffered, incomplete, and shredded: The challenges of reading an imperfect stratigraphic record. *Journal of Geophysical Research: Earth Surface*, *125*(3), e2019JF005079. doi: https://doi.org/10.1029/2019JF005079

Van Dijk, M., Kleinhans, M. G., Postma, G., & Kraal, E. (2012). Contrasting morphodynamics in alluvial fans and fan deltas: effect of the downstream boundary. *Sedimentology*, *59*(7), 2125-2145.

Van Dijk, M., Postma, G., & Kleinhans, M. G. (2009). Autocyclic behaviour of fan deltas: an analogue experimental study. *Sedimentology*, *56*(5), 1569-1589.

Vincent, L., Eaton, B. C., Leenman, A. S., & Jakob, M. (In revision). Secondary geomorphic processes and their influence on alluvial fan morphology, channel behaviour and flood hazards. *Submitted to Journal of Geophysical Research, Earth Surface*. doi: DOI:10.1002/essoar.10507644.1

Whipple, K. X., Parker, G., Paola, C., & Mohrig, D. (1998). Channel dynamics, sediment transport, and the slope of alluvial fans: Experimental study. *Journal of Geology*, *106*(6), 677-693.

Wilcock, P. R., & Crowe, J. C. (2003). Surface-based transport model for mixed-size sediment. *Journal of Hydraulic Engineering*, *129*(2), 120–128.

Wilcock, P. R., & Kenworthy, S. T. (2002). A two-fraction model for the transport of sand/gravel mixtures. *Water Resources Research*, *38*(10), 12–1.

Wong, M., & Parker, G. (2006). Reanalysis and correction of bed-load relation of Meyer-Peter and Müller using their own database. *Journal of Hydraulic Engineering*, *132*(11), 1159–1168.

Woods, S. W., MacDonald, L. H., & Westbrook, C. J. (2006). Hydrologic interactions between an alluvial fan and a slope wetland in the central Rocky Mountains, USA. *Wetlands*, *26*(1), 230-243.

Yalin, M. S. (1971). *Theory of hydraulic models.* Macmillan International Higher Education.

Yumuang, S. (2006). 2001 debris flow and debris flood in Nam Ko area, Phetchabun province, central Thailand. *Environmental Geology*, *51*(4), 545–564.